

Oceanic non-Kolmogorov optical turbulence and spherical wave propagation

JIN-REN YAO,^{1,3} HAN-TAO WANG,¹ HUA-JUN ZHANG,¹ JIAN-DONG CAI,¹ MING-YUAN REN,¹ YU ZHANG,^{1,*} AND OLGA KOROTKOVA,²

¹*School of Physics, Harbin Institute of Technology, Harbin, 150001, China*

²*Department of Physics, University of Miami, Coral Gables, FL 33146, USA*

³*jinry@yahoo.com*

**Corresponding author: zhangyuhitphy@163.com*

**This paper has been published in Optics Express <https://doi.org/10.1364/OE.409498>. This PDF you are reading is a further modified version where we adjusted few words.*

Abstract: Light propagation in turbulent media is conventionally studied with the help of the spatio-temporal power spectra of the refractive index fluctuations. In particular, for natural water turbulence several models for the spatial power spectra have been developed based on the classic, Kolmogorov postulates. However, as currently widely accepted, non-Kolmogorov turbulent regime is also common in the stratified flow fields, as suggested by recent developments in atmospheric optics. Until now all the models developed for the non-Kolmogorov optical turbulence were pertinent to atmospheric research and, hence, involved only one advected scalar, e.g., temperature. We generalize the oceanic spatial power spectrum, based on two advected scalars, temperature and salinity concentration, to the non-Kolmogorov turbulence regime, with the help of the so-called "Upper-Bound Limitation" and by adopting the concept of spectral correlation of two advected scalars. The proposed power spectrum can handle general non-Kolmogorov, anisotropic turbulence but reduces to Kolmogorov, isotropic case if the power law exponents of temperature and salinity are set to 11/3 and anisotropy coefficient is set to unity. To show the application of the new spectrum, we derive the expression for the second-order mutual coherence function of the spherical wave and examine its coherence radius (in both scalar and vector forms) to characterize the turbulent disturbance. Our numerical calculations show that the statistics of the spherical wave vary substantially with temperature and salinity non-Kolmogorov power law exponents and temperature-salinity spectral correlation coefficient. The introduced spectrum is envisioned to become of significance for theoretical analysis and experimental measurements of non-classic natural water double-diffusion turbulent regimes.

© 2021 Optical Society of America under the terms of the [OSA Open Access Publishing Agreement](#)

1. Introduction

The stable temperature stratification and the stable salinity stratification in marine environment may be disturbed by the velocity field, which results in the inhomogeneous spatio-temporal distribution of temperature and salinity, and hence leads to the spatio-temporal fluctuations of refractive-index. We name such refractive-index fluctuations as oceanic optical turbulence [1]. Besides, the oceanic optical turbulence could also be driven by other factors like winds, gravity and vertical currents. The Oceanic Turbulence Optical Power Spectrum (OTOPS) being the Fourier transform of the spatial covariance function of the refractive index provides an essential tool for characterizing the spatial statistics of any order for stationary light fields propagating through the natural waters. Within the last two decades, the oceanic power spectrum model developed in [2] based on Kolmogorov turbulence theory resulted, with the help of the Rytov and the extended Huygens-Fresnel methods, in a number of theoretical predictions relating to light interaction with turbulent waters. In particular, evolution of the spectral density [3], the

spectral shifts [4], the polarimetric [5] and coherence [6] changes and propagation of several other 2nd-order and 4th-order statistics [7–10] have been revealed. The theory has also benefited a number of underwater applications, such as the oceanic Light Detection and Ranging (Lidar) [11] systems, underwater optical communications [12–14], and underwater imaging [15].

Since the oceanic optical turbulence is governed by two scalar fields, temperature and salinity concentration, the OTOPS is approximately expressed as a linear combination of temperature power spectrum, salinity power spectrum and their co-spectrum [2]. Therefore OTOPS contains many parameters, such as the Kolmogorov scale η , the Prandtl number Pr , the Schmidt number Sc , as well as the dissipation rates of temperature, salinity, and kinetic energy, χ_T , χ_S , and ε , respectively, substantially complicating the predictions for the light - oceanic turbulence interactions.

The OTOPS model of [2] and its derivatives [16, 17] were all based on the first of the four models (called below H1) for a single-scalar turbulent advection developed by Hill [18]. An alternative model for the Kolmogorov oceanic optical turbulence has been recently obtained in [19–22] by numerically fitting model 4 of the Hill's paper (called below H4) [18]. The H4-based models are more precise than the H1-based models in high spatial frequency region, and, hence, have advantages in oceanic cases with the wide-ranged Prandtl/Schmidt numbers [21, 23]. *All the aforementioned OTOPS models are based on the Kolmogorov theory having a constant power law $-11/3$, and the co-spectra in these models are obtained by analogy with a single scalar (temperature or salinity) spectrum.*

Kolmogorov theory relies on several assumptions including the homogeneous and isotropic nature of turbulent eddies. Such regime is clearly not universal, since it is not being able to account for several anomalous phenomena such as ramp-cliff signature and unusual scaling exponent (e. g. [24]). Over the past 30 years, several experiments have revealed the presence of non-classic atmospheric optical turbulence [25–30]. The power spectrum model of the non-Kolmogorov turbulence advected by a single scalar and light interaction with such turbulence have been widely discussed in atmospheric optics literature [31–39]. *However, it is our understanding that a comprehensive non-Kolmogorov model for oceanic waters does not exist.*

Non-Kolmogorov phenomena, as a result of inadequate rate of energy cascade, are common in underdeveloped or vertically suppressed atmospheric turbulence, and do appear in stratified marine environment. In two oceanic experiments by Ichiye [40] and by Pochapsky and Malone [41] the non-Kolmogorov fluctuations of temperature and salinity have been observed. In the Ichiye's measurement, the power law of temperature and salinity were between $-11/3$ and -5 , which was interpreted as the result of oceanic stratification. In Pochapsky and Malone measurement, a -4 power law was obtained [41].

On considering the results of these oceanic turbulence measurements and the practical need for light propagation predictions made in various oceanic turbulence regimes, *we set the aim for this paper to develop an OTOPS that extends the model suggested in [21, 22] to non-Kolmogorov regime.* This requires (I) developing the non-Kolmogorov temperature/salinity spectrum which is applicable for the marine environment with the wide-ranged Prandtl/Schmidt numbers, and (II) deriving the temperature-salinity co-spectrum which can not be directly obtained by analogy with a single-scalar spectrum, since the power law exponents of the two advected scalars can be generally different.

The paper is organized as follows: using a non-Kolmogorov structure function, we derive the non-Kolmogorov temperature and salinity spectra based on the H4-based model (Section 2.1); using the Upper-Bound limitation, we develop a temperature-salinity co-spectrum (Section 2.2); on combining the results for the temperature spectrum, the salinity spectrum and the co-spectrum, we introduce a non-Kolmogorov OTOPS (NK-OTOPS) model (Section 3); we apply the NK-OTOPS model for the analysis of the spherical wave propagation (Section 4); and we summarize the obtained results (Section 5).

2. Temperature/salinity spectra and their co-spectrum in ocean

The OTOPS is composed of temperature spectrum, salinity spectrum, and temperature-salinity co-spectrum. In this section, we will derive the non-Kolmogorov temperature/salinity spectra (Section 2.1) and the temperature-salinity co-spectrum (Section 2.2).

2.1. Non-Kolmogorov temperature/salinity spectra

We begin by recalling the H4-based temperature/salinity spectrum that has been developed for Kolmogorov case in [21]. By comparing its structure function with the Kolmogorov structure function, we will first obtain its structure constant C_i^2 and its inner scale l_{i0} . Then, the H4-based spectrum will be modified into a non-Kolmogorov spectrum.

2.1.1. A. H4-based temperature/salinity spectrum

Here the H4-based temperature/salinity spectrum [21] is re-organized as

$$\Phi_i(\kappa) = C_k C_i^2 \kappa^{-11/3} g_i(\kappa\eta), \text{ with } i \in \{T, S\}, \quad (1)$$

where κ is the wavenumber [m^{-1}]; C_i^2 is the structure constant (dimensionless); C_k is a dimensionless constant given by

$$C_k C_i^2 = \frac{\beta \varepsilon^{-1/3} \chi_i}{4\pi}, \quad (2)$$

β is the Obukhov-Corrsin constant (non-dimensional); ε is the dissipation rate of kinetic energy [m^2s^{-3}]; χ_i is the ensemble-averaged variance dissipation rate of temperature or salinity ($i \in \{T, S\}$) with unit K^2s^{-1} or g^2s^{-1} ; the non-dimensional function $g_i(x)$ is

$$g_i(x) = \sum_{j=0}^2 a_j x^{b_j} \exp\left(-174.90 x^2 c_i^{0.96}\right), \quad (3)$$

with

$$\{a_j\} = \{1, 21.61c_i^{0.02}, -18.18c_i^{0.04}\}, \quad (4)$$

$$\{b_j\} = \{0, 0.61, 0.55\}, \quad (5)$$

$$c_i = a^{4/3} \beta \text{Pr}_i^{-1}, \quad (6)$$

where Pr_T and Pr_S are the temperature Prandtl number and salinity Schmidt number, respectively, a is a constant and generally equals 0.072, and β is the Obukhov-Corrsin constant being approximately to 0.72 [18].

2.1.2. B. Structure constant C_i^2 and inner scale l_{i0}

Structure constant C_i^2 and inner scale l_{i0} are the key parameters in the turbulence structure function, and they will be obtained by comparing the corresponding structure function in the Kolmogorov case.

The structure function of Eq.(1) is

$$\begin{aligned} D_i(R) &= 8\pi \int_0^\infty \kappa^2 \Phi_i(\kappa) \left(1 - \frac{\sin \kappa R}{\kappa R}\right) d\kappa \\ &= \beta \varepsilon^{-1/3} \chi_i \eta^{2/3} \sum_{j=0}^2 a_j \left\{ \left(174.90 c_i^{0.96}\right)^{\frac{1}{3} - \frac{b_j}{2}} \Gamma\left(-\frac{1}{3} + \frac{b_j}{2}\right) \right. \\ &\quad \left. \left[1 - {}_1F_1\left(-\frac{1}{3} + \frac{b_j}{2}, \frac{3}{2}, -\frac{R^2}{4 \times 174.90 c_i^{0.96} \eta^2}\right)\right] \right\}, \end{aligned} \quad (7)$$

where $\Gamma(\cdot)$ is a Gamma function, and ${}_1F_1(\cdot, \cdot, \cdot)$ is a generalized hyper-geometric function. For Kolmogorov turbulence advected by a single scalar (temperature or salinity), the structure function is (Chapter 3 of [42]):

$$D_i(R) = \begin{cases} C_i^2 l_{i0}^{-4/3} R^2 & R \ll l_{i0}, \\ C_i^2 R^{2/3} & R \gg l_{i0}, \end{cases} \quad \text{with } i \in \{T, S\}. \quad (8)$$

By comparing Eqs. (7) and (8), and in combining with Eq. (2), we get the dimensionless constant

$$C_k = \frac{-\Gamma(11/6) 2^{2/3}}{4\pi\Gamma(-1/3)\Gamma(3/2)} \approx 0.033, \quad (9)$$

the structure constant

$$C_i^2 = -\beta\varepsilon^{-1/3} \chi_i \Gamma(-1/3) \frac{\Gamma(3/2)}{\Gamma(11/6)} 2^{-2/3}, \quad (10)$$

and the inner scale

$$l_{i0} = \eta/T(c_i), \quad (11)$$

where

$$T(c_i) = \left\{ \pi C_k \sum_{j=0}^2 a_j \left[\left(174.90 c_i^{0.96} \right)^{-\frac{b_j}{2} - \frac{2}{3}} \left(\frac{3b_j - 2}{9} \right) \Gamma\left(\frac{3b_j - 2}{6}\right) \right] \right\}^{3/4}, \quad (12)$$

with a_j , b_j and c_i defined in Eqs. (4)-(6), respectively.

2.1.3. C. Non-Kolmogorov case

Now, we modify Eq. (1) to a non-Kolmogorov spectrum. Following the modification in atmospheric optics [31, 32, 43], we add two adaptive functions $A(\alpha_i)$ and $h(\alpha_i, c_i)$ to Eq. (1),

$$\Phi_i(\kappa, \alpha_i) = A(\alpha_i) C_i^2 \kappa^{-\alpha_i} g_i(\kappa\eta'), \quad (13)$$

with

$$\eta' = \frac{\eta}{h(\alpha_i, c_i)}, \quad (14)$$

where $A(\alpha_i)$ is a variable factor similar to the ‘ $A(\alpha)$ ’ in [31], $h(\alpha_i, c_i)$ is a scaling function similar to the ‘ $c(\alpha)$ ’ in [31], it adjusts the location of viscous range on κ -axis. *Expressions of $A(\alpha_i)$ and $h(\alpha_i, c_i)$ are derived as follows.*

The structure function of Eq.(13) is

$$\begin{aligned} D_i(R, \alpha_i) &= 8\pi \int_0^\infty \kappa^2 \Phi_i(\kappa, \alpha_i) \left(1 - \frac{\sin \kappa R}{\kappa R} \right) d\kappa \\ &= 4\pi C_i^2 A(\alpha_i) \eta'^{\alpha-3} \sum_{j=0}^2 a_j \left\{ \left(174.90 c_i^{0.96} \right)^{-\frac{3-b_j+\alpha_i}{2}} \Gamma\left(\frac{3+b_j-\alpha_i}{2}\right) \right. \\ &\quad \left. \left[{}_1F_1\left(\frac{3+b_j-\alpha_i}{2}, \frac{3}{2}, -\frac{R^2}{4(174.90 c_i^{0.96}) \eta'^2}\right) \right] \right\}, \end{aligned} \quad (15)$$

and the non-Kolmogorov structure function [31, 32] is

$$D_i(R, \alpha_i) = \begin{cases} C_i^2 l_{i0}^{\alpha_i-5} R^2 & R \ll l_{i0}, \\ C_i^2 R^{\alpha_i-3} & R \gg l_{i0}, \end{cases} \quad (16)$$

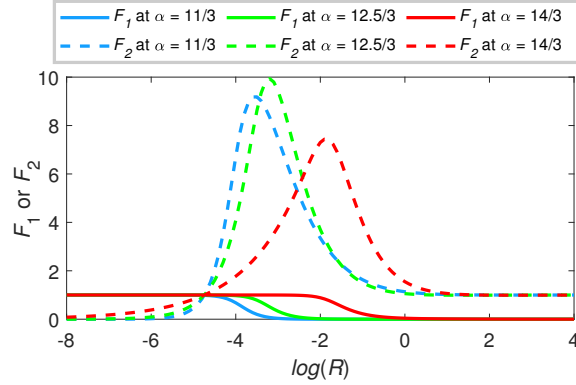


Fig. 1. Functions $F_1(R)$ and $F_2(R)$ in Eq. (20). The solid curves represent F_1 , and the dashed curves represent F_2 . R has a unit [m], and the functions $F_1(R)$, $F_2(R)$ are dimensionless.

where C_i^2 and l_{i0} have been obtained in Eqs. (10) and (11), respectively. By comparing Eq. (15) with Eq. (16), we have

$$A(\alpha_i) = \frac{\Gamma(\alpha_i - 1)}{4\pi^2} \cos\left(\frac{\pi\alpha_i}{2}\right), \quad (17)$$

and

$$h(\alpha_i, c_i) = G(\alpha_i, c_i) T_i(c_i), \quad (18)$$

with

$$G(\alpha_i, c_i) = \left[\pi A(\alpha_i) \sum_{j=0}^2 a_j (174.90 c_i^{0.96})^{\frac{-5-b_j+\alpha_i}{2}} \left(\frac{3+b_j-\alpha_i}{3}\right) \Gamma\left(\frac{3+b_j-\alpha_i}{2}\right) \right]^{\frac{1}{\alpha_i-5}}, \quad (19)$$

$T_i(c_i)$ has been given in Eq. (12). When $\alpha_i = 11/3$, we have $A(11/3) = C_k \approx 0.033$ and $h(11/3, c_i) = 1$. Hence, the non-Kolmogorov spectrum Eq. (13) can degenerate into the traditional Kolmogorov model Eq. (1).

To show the consistency between the proposed non-Kolmogorov spectrum Eq. (13) and the non-Kolmogorov structure function Eq. (16), we plot the following two functions in Fig. 1,

$$\begin{cases} F_1(R) = \left(C_i^2 l_{i0}^{\alpha_i-5} R^2\right)^{-1} 8\pi \int_0^\infty \kappa^2 \Phi_i(\kappa) \left(1 - \frac{\sin \kappa R}{\kappa R}\right) d\kappa, \\ F_2(R) = \left(C_i^2 R^{\alpha_i-3}\right)^{-1} 8\pi \int_0^\infty \kappa^2 \Phi_i(\kappa) \left(1 - \frac{\sin \kappa R}{\kappa R}\right) d\kappa. \end{cases} \quad (20)$$

It shows $F_1(R \rightarrow 0) = 1$ and $F_2(R \rightarrow \infty) = 1$, which indicates that the modified non-Kolmogorov spectrum Eq.(13) agrees well with the asymptotic formula Eq. (16).

Equation (13) together with Eqs. (14), (17) and (18) constitute the main results of this section. They give the non-Kolmogorov spectrum of oceanic temperature/salinity turbulence, and the proposed spectrum agrees well with the widely accepted asymptotic structure function. It must be noticed that parameter c_i is related to Prandtl/Schmidt number in Kolmogorov case but this definite relation is broken in non-Kolmogorov cases because of the presence of inhomogeneous, anisotropic and/or underdeveloped turbulence. In what follows, we consider c_i as a direct parameter, and set its range in Appendix I.

2.2. Non-Kolmogorov temperature-salinity co-spectrum

In the Kolmogorov case the models of temperature-salinity co-spectrum have been obtained by analogy with the single scalar (temperature/salinity) spectrum [2, 16, 19, 21] but such an analogy is unavailable if the exponents of temperature and salinity spectra are different. Hence, for the non-Kolmogorov case, the temperature-salinity co-spectrum should be obtained by other means. In this section, we will derive the temperature-salinity co-spectrum based on the Upper-Bound Limitation [44–46] and the concept of spectral correlation [47].

As proven in Section 5.2.5 of [44], the Upper-Bound Limitation gives the relation between scalar spectra ϕ_T , ϕ_S and their co-spectrum ϕ_{TS} :

$$0 \leq \phi_{TS}(\kappa) \leq [\phi_T(\kappa) \phi_S(\kappa)]^{1/2}. \quad (21)$$

In Ref. [48] the Upper-Bound Limitation was extended to three-dimensional case:

$$0 \leq \Phi_{TS}(\kappa, \alpha_T, \alpha_S) \leq [\Phi_T(\kappa, \alpha_T) \Phi_S(\kappa, \alpha_S)]^{1/2}. \quad (22)$$

By adopting the concept of spectral correlation [47, 49], and combining Eq.(13) with Eq. (22), we obtain the temperature-salinity co-spectrum as

$$\begin{aligned} \Phi_{TS}(\kappa, \alpha_T, \alpha_S) &= \gamma_{ST}(\kappa\eta) [\Phi_T(\kappa, \alpha_T) \Phi_S(\kappa, \alpha_S)]^{1/2} \\ &= \gamma_{ST}(\kappa\eta) A_{TS}(\alpha_T, \alpha_S) C_{TS}^2 \kappa^{-(\alpha_T + \alpha_S)/2} g_{TS}(\kappa\eta), \end{aligned} \quad (23)$$

with

$$C_{TS}^2 = \left(C_T^2 C_S^2 \right)^{1/2}, \quad (24)$$

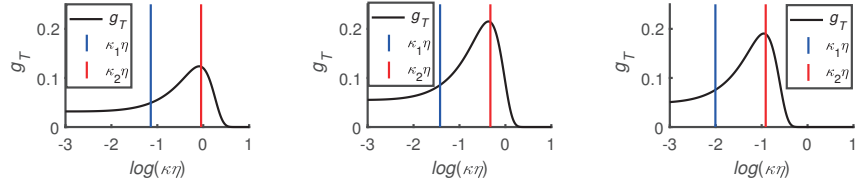
$$A_{TS}(\alpha_T, \alpha_S) = [A(\alpha_T) A(\alpha_S)]^{1/2}, \quad (25)$$

$$g_{TS}(\kappa\eta) = \left[g_T \left(\frac{\kappa\eta}{h(\alpha_T, c_T)} \right) g_S \left(\frac{\kappa\eta}{h(\alpha_S, c_S)} \right) \right]^{1/2}, \quad (26)$$

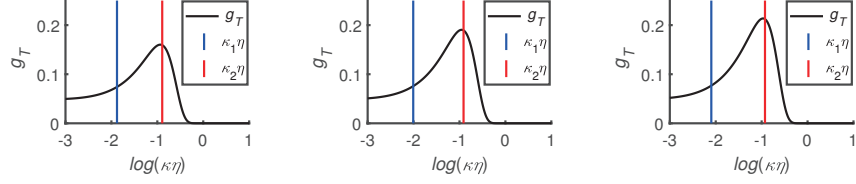
where $\gamma_{ST}(\kappa\eta)$ is a correlation factor describing the degree of correlation between temperature spectrum and salinity spectrum, and $0 \leq \gamma_{ST}(\kappa\eta) \leq 1$. When $\gamma_{ST} = 1$, Eq. (23) refers to a fully correlated co-spectrum; when $\gamma_{ST} = 0$, Eq.(23) refers to an uncorrelated co-spectrum that $\Phi_{TS} = 0$; when $0 < \gamma_{ST} < 1$, the co-spectrum is partially correlated. Details about partially correlated co-spectrum are given as follows.

According to the concept of spectral correlation [47, 48], temperature fluctuation T' and salinity fluctuation S' are highly correlated if they are both driven by eddy diffusion, but the correlation will be broken down if T' is driven by temperature molecular diffusion. Hence, the following should hold [50]:

- When κ belongs to **the inertial-convective range of Φ_T** (i.e. $g_T \propto \kappa^0$), the salinity spectrum is generally in its inertial-convective range [51]. Thus, both T' and S' are governed by eddy diffusion, and they have a **high correlation**, i.e. $\gamma_{ST} = \gamma_{\max} \leq 1$.
- When κ belongs to **the viscous-convective range of Φ_T** (i.e. $g_T \propto \kappa^{2/3}$), T' is consumed by viscosity but S' is still governed by eddy diffusion. The **correlation** begins to decrease in this range, and it has been observed in [52] that correlation decreases monotonically. Hence, we have $d\gamma_{ST}/d\kappa \leq 0$.
- When κ belongs to **the viscous-diffusive range of Φ_T** (i.e. g_T decreases fast with κ), T' is primarily depleted by temperature molecular diffusion, which leads to a **very low correlation** between T' and S' , i.e. $\gamma_{ST} \approx 0$.



(a) $\alpha_T = 11/3$, $c_T = 2.2 \times 10^{-3}$; (b) $\alpha_T = 12.5/3$, $c_T = 2.2 \times 10^{-3}$; (c) $\alpha_T = 14/3$, $c_T = 2.2 \times 10^{-3}$;



(d) $\alpha_T = 14/3$, $c_T = 3.6 \times 10^{-3}$; (e) $\alpha_T = 14/3$, $c_T = 2.2 \times 10^{-3}$; (f) $\alpha_T = 14/3$, $c_T = 1.5 \times 10^{-3}$;

Fig. 2. The locations of $\kappa_1\eta$ (‘|’) and $\kappa_2\eta$ (‘|’) defined by Eqs. (29)-(30). Here the horizontal and vertical axes are all dimensionless.

Thus the value of correlation parameter $\gamma_{ST}(\kappa\eta)$ obeys the following constraints:

$$\begin{cases} \gamma_{ST}(\kappa\eta) = \gamma_{\max} \leq 1 & \text{when } \kappa \ll \kappa_1, \\ \gamma_{ST}(\kappa\eta) \in [0, \gamma_{\max}] \text{ and } d\gamma_{ST}/d\kappa \leq 0 & \text{when } \kappa_1 \ll \kappa \ll \kappa_2, \\ \gamma_{ST}(\kappa\eta) \approx 0 & \text{when } \kappa \gg \kappa_2, \end{cases} \quad (27)$$

where κ_1 defines the transition between inertial-convective and viscous-convective ranges of Φ_T , κ_2 defines the transition between viscous-convective and viscous-diffusive ranges of Φ_T . According to [18], we have the following defining relations for κ_1 and κ_2 in H4-based non-Kolmogorov model:

$$\frac{\kappa_1\eta}{h(\alpha_T, c_T)} = a, \quad (28)$$

and

$$\frac{\kappa_2\eta}{h(\alpha_T, c_T)} = \left(\frac{3a^{4/3}}{22Qc_T} \right)^{1/2}, \quad (29)$$

where η is the Kolmogorov scale; $h(\alpha_T, c_T)$ is the non-Kolmogorov scaling function given in Eq. (18); a is a constant approximating to 0.072 [2]; Q is another constant about 2.35 [2]; and c_T has been given in Eq. (6). The locations of $\kappa_1\eta$ and $\kappa_2\eta$ are marked by ‘|’ and ‘|’ in Fig.2, respectively, and ‘—’ refers to g_T . It shows that $\kappa_1\eta$ and $\kappa_2\eta$ mark the transitions between different ranges very well.

For mathematical simplicity of discussion, we suppose that the correlation factor in *fully correlated* case is

$$\gamma_{ST} = 1, \quad (30)$$

and in *partially correlated* case it takes form

$$\gamma_{ST}(\kappa\eta) = \frac{1 - \tanh \{ [\log(\kappa\eta) - (\log(\kappa_1\eta) + \log(\kappa_2\eta)) / 2] \rho \}}{2} \gamma_{\max}, \quad (31)$$

with

$$\rho = \frac{2p}{\log(\kappa_2\eta) - \log(\kappa_1\eta)}, \quad \gamma_{\max} = 1, \quad (32)$$

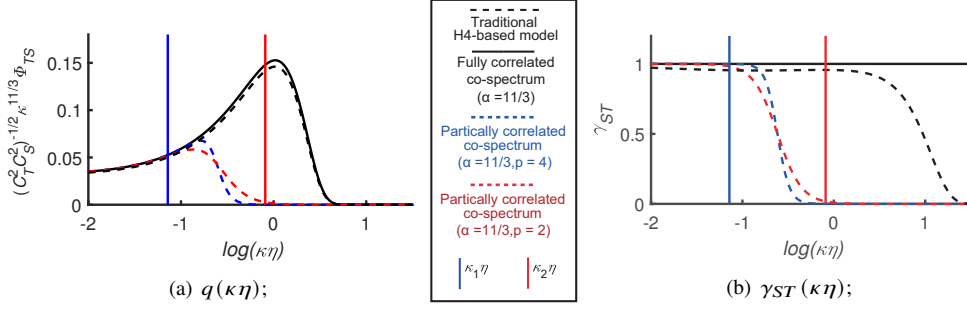


Fig. 3. Comparing (a) the non-dimensional function $q(\kappa\eta)$ and (b) the correlation factor $\gamma_{ST}(\kappa\eta)$ corresponding to the proposed co-spectrum with these corresponding to conventional co-spectrum [21]. Values of parameters are listed in Appendix II. The unit of the vertical axis of (a) is $[m^{(\alpha_T+\alpha_S)/2-11/3}]$. γ_{ST} and $\kappa\eta$ are dimensionless.

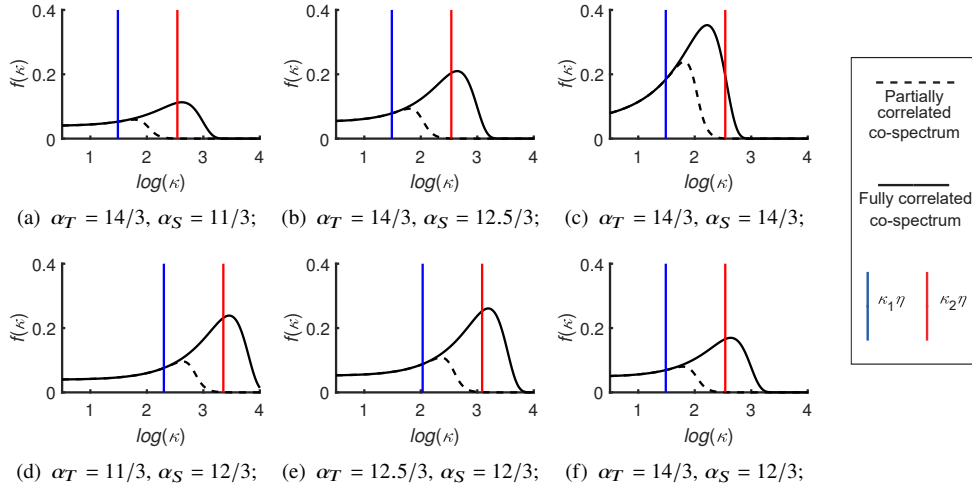


Fig. 4. The curves of the dimensionless function $f(\kappa) = \kappa^{(\alpha_T+\alpha_S)/2}(C_T^2 C_S^2)^{-1/2} \Phi_{TS}$ with different values of α_T and α_S . Here κ is dimensionless.

where p controls the transition speed of γ_{ST} from γ_{\max} to 0.

In Figure 3 we compare Eq. (23) with the conventional co-spectrum [21] limiting ourselves to *Kolmogorov case* ($\alpha_S = \alpha_T = 11/3$). Fig. 3(a) shows non-dimensional function $q(\kappa\eta) = (C_T^2 C_S^2)^{-1/2} \kappa^{11/3} \Phi_{TS}$ varying with $\log(\kappa\eta)$, where ‘---’ refers to the traditional co-spectrum [21]; ‘—’ refers to the proposed co-spectrum in Eq. (23) with a full correlation $\gamma_{ST} = 1$; the curves ‘- - -’ and ‘- - -’ refer to the partially correlated co-spectra with $p = 4$ and $p = 2$, respectively. The vertical lines ‘|’ and ‘|’ mark the locations of $\kappa_1\eta$ and $\kappa_2\eta$, respectively. With similar legends, Fig. 3(b) shows correlation factor γ_{ST} varying with $\log(\kappa\eta)$ [53].

Figure 3 shows that: *for the Kolmogorov case* and in comparison with the conventional co-spectrum [21], the proposed partially correlated co-spectrum has a higher correlation in the temperature inertial-convective range ($\kappa \ll \kappa_1$), a lower correlation in the temperature viscous-convective range ($\kappa_1 \ll \kappa \ll \kappa_2$), and also a low correlation in the temperature viscous-diffusive range ($\kappa \gg \kappa_2$). Furthermore, Fig.3 (a) indicates that the proposed fully correlated co-spectrum tends to the conventional co-spectrum when $\alpha_T = \alpha_S = 11/3$.

To examine the co-spectrum *in non-Kolmogorov case*, and to verify its de-correlation within temperature viscous-convective range, we plot \log of non-dimensional function $f(\kappa) = \kappa^{(\alpha_T + \alpha_S)/2} (C_T^2 C_S^2)^{-1/2} \Phi_{TS}$ in Fig.4, and compare the fully correlated co-spectrum ('—') with the partially correlated co-spectrum ('---') at $p = 3$. Same as before, $\kappa_1 \eta$ and $\kappa_2 \eta$ are marked by '↓' and '↑', respectively. It is shown that the proposed co-spectrum has low correlation in the temperature inertial-convective range, as expected. This agrees with Eq. (27).

Thus we have obtained a temperature-salinity co-spectrum with a non-Kolmogorov power law $(\alpha_T + \alpha_S)/2$ and a flexible correlation factor γ_{ST} [see Eq. (23)]. If $\gamma_{ST} = 1$, the proposed co-spectrum is fully correlated, and it approximately reduces to the conventional co-spectrum when $\alpha_T = \alpha_S = 11/3$; if $\gamma_{ST} = 0$, the proposed co-spectrum is uncorrelated, i.e. $\Phi_{TS} = 0$; if γ_{ST} obeys Eq. (31), the proposed co-spectrum is partially correlated. As we expected, the new co-spectrum model has a power law between α_T and α_S ; if the temperature and salinity fields are both Kolmogorov ($\alpha_T = \alpha_S = 11/3$), the co-spectrum is also Kolmogorov ($\alpha_{TS} = 11/3$).

3. OTOPS with anisotropy and non-Kolmogorov power law

In general, the oceanic refractive-index fluctuation n' is approximately given by a linear combination of temperature fluctuation T' and salinity fluctuation S' [2, 22, 54]:

$$n' \approx n'_T T' + n'_S S', \quad (33)$$

with

$$n'_T = \frac{dn'}{dT'}, \quad n'_S = \frac{dn'}{dS'}. \quad (34)$$

This implies that the spectrum of n' is approximately given by linear combination

$$\Phi_{n0}(\kappa) = n'^2_T \Phi_T(\kappa) + n'^2_S \Phi_S(\kappa) + 2n'_T n'_S \Phi_{TS}(\kappa), \quad (35)$$

where Φ_T is the temperature spectrum, Φ_S is the salinity spectrum, and Φ_{TS} is the temperature-salinity co-spectrum. On incorporating Eqs. (13) and (23) into Eq. (35), we obtain the following expression for the NK-OTOPS:

$$\begin{aligned} \Phi_{n0}(\kappa) &= n'^2_T \Phi_T(\kappa) + n'^2_S \Phi_S(\kappa) + 2n'_T n'_S \gamma_{ST}(\kappa \eta) \sqrt{\Phi_T(\kappa) \Phi_S(\kappa)} \\ &= n'^2_T C_T^2 A(\alpha_T) \kappa^{-\alpha_T} g_T(\kappa \eta / h_T) + n'^2_S C_S^2 A(\alpha_S) \kappa^{-\alpha_S} g_S(\kappa \eta / h_S) + 2n'_T n'_S \gamma_{ST} \\ &\quad \left(C_T^2 C_S^2 \right)^{1/2} [A(\alpha_T) A(\alpha_S)]^{1/2} \kappa^{-(\alpha_T + \alpha_S)/2} [g_T(\kappa \eta / h_T) g_S(\kappa \eta / h_S)]^{1/2}. \end{aligned} \quad (36)$$

with

$$h_T = h(\alpha_T, c_T), \quad h_S = h(\alpha_S, c_S). \quad (37)$$

To make the developed NK-OTOPS more physical we now implement the finite outer-scale cut-off and extend it to the anisotropic case. To obtain the first extension we use the filter function with exponential form [20, 55]:

$$\Phi_{n1}(\kappa) = \left[1 - \exp\left(-\frac{\kappa^2}{\kappa_0^2}\right) \right] \Phi_{n0}(\kappa), \quad (38)$$

where κ_0 is the outer-scale cut-off wavenumber defined by $\kappa_0 \approx 4\pi/L_0$ with L_0 (m) representing the outer scale. Further the *anisotropic* NK-OTOPS can be obtained on following [56] as:

$$\Phi_{n2}(\kappa) = \mu^2 \Phi_{n1}(\kappa_{\text{iso}}), \quad (39)$$

where μ is the anisotropy parameter, $\boldsymbol{\kappa}$ is the three-dimensional wavenumber, and $\boldsymbol{\kappa}_{\text{iso}}$ is a isotropizing transformation of $\boldsymbol{\kappa}$:

$$\boldsymbol{\kappa} = (\kappa_x, \kappa_y, \kappa_z)^\top, \quad \boldsymbol{\kappa}_{\text{iso}} = (\mu\kappa_x, \mu\kappa_y, \kappa_z)^\top, \quad \kappa_{\text{iso}} = |\boldsymbol{\kappa}_{\text{iso}}|, \quad (40)$$

T is denoting vector transpose.

Thus in this section, a non-Kolmogorov OTOPS (NK-OTOPS) is given in Eq. (36), while its extended form for outer-scaled and anisotropic cases are presented by Eqs. (38) and (39), respectively.

4. Spherical wave propagation in oceanic optical turbulence

As an example of applying the NK-OTOPS, and on taking into account the significance of the spherical wave statistics for the extended Huygens-Fresnel principle, we will calculate and analyze the 2nd-order statistics of a spherical wave. In particular, in Section 4.1, the wave structure function (WSF) of a spherical wave in oceanic turbulence will be derived; in Section 4.2, the vector and scalar versions of the coherence radius will be defined and examined; and in Section 4.3, the co-effect of temperature and salinity on spherical wave's propagation will be discussed by calculating its scalar coherence radius varying with α_T , α_S , c_T and c_S .

4.1. 2nd-order statistical moments and wave structure function of spherical wave

4.1.1. A. 2nd-order statistical moments

We will first derive the 2nd-order statistical moment of a spherical wave propagating in the non-Kolmogorov oceanic optical turbulence. According to Eq. (59) of chapter 5 in [42], for horizontal channels (along y-axis) this quantity has form:

$$E_{2_h}(\mathbf{r}_1, \mathbf{r}_2) = \frac{2\pi k^2}{n_0^2} \int_0^L d\eta \int \int_{-\infty}^{+\infty} d^2\boldsymbol{\kappa} \cdot \Phi_{n2}(\boldsymbol{\kappa}) \exp \left[i\boldsymbol{\kappa} (\gamma \mathbf{r}_1 - \gamma^* \mathbf{r}_2) - \frac{i\kappa^2}{2k} (\gamma - \gamma^*) (L - \eta) \right], \quad (41)$$

with

$$\boldsymbol{\kappa} = (\kappa_x, \kappa_z)^\top, \quad \mathbf{r}_1 = (r_{1x}, r_{1z})^\top, \quad \mathbf{r}_2 = (r_{2x}, r_{2z})^\top, \quad (42)$$

where L is the propagation distance from the source plane, k is the wavenumber defined as $2\pi n_0/\lambda$, n_0 being the average refractive-index, Φ_{n2} is the anisotropic NK-OTOPS as given by Eq. (39). For a spherical wave, $\gamma = \gamma^* = 1$. On assuming that

$$\boldsymbol{\kappa}_t = (\mu\kappa_x, \kappa_z)^\top, \quad \mathbf{r}_{1_iso} = (r_{1x}/\mu, r_{1z})^\top, \quad \mathbf{r}_{2_iso} = (r_{2x}/\mu, r_{2z})^\top, \quad (43)$$

and combining Eq. (39) with Eq. (41), we get

$$\begin{aligned} E_{2_h}(\mathbf{r}_1, \mathbf{r}_2) &= \frac{2\pi k^2}{n_0^2 \mu} \int_0^L d\eta \int \int_{-\infty}^{+\infty} d^2\boldsymbol{\kappa}_t \cdot \mu^2 \Phi_{n1}(\boldsymbol{\kappa}_t) \exp [i\boldsymbol{\kappa}_t (\mathbf{r}_{1_iso} - \mathbf{r}_{2_iso})] \\ &= \frac{4\pi^2 k^2 \mu L}{n_0^2} \int_0^{+\infty} d\kappa_t \cdot \kappa_t \Phi_{n1}(\kappa_t) J_0 [\kappa_t |\mathbf{r}_{1_iso} - \mathbf{r}_{2_iso}|], \end{aligned} \quad (44)$$

where Φ_{n1} is the outer-scaled NK-OTOPS in Eq. (38). On setting $\boldsymbol{\rho} = \mathbf{r}_1 - \mathbf{r}_2$, we find that the 2nd-order statistical moment of a spherical wave along a horizontal channel (along the y-axis) becomes

$$E_{2_h}(\boldsymbol{\rho}) = \frac{4\pi^2 k^2 \mu L}{n_0^2} \int_0^{+\infty} d\kappa_t \cdot \kappa_t \Phi_{n1}(\kappa_t) J_0 \left[\kappa_t \sqrt{\mu^{-2} \rho_x^2 + \rho_z^2} \right], \quad (45)$$

where

$$\kappa_t = |(\mu\kappa_x, \kappa_z)^\top|. \quad (46)$$

Similarly, the 2nd-order statistical moment of a spherical wave in a vertical channel (along the z-axis) becomes

$$E_{2_{-v}}(\boldsymbol{\rho}) = \frac{4\pi^2 k^2 L}{n_0^2} \int_0^{+\infty} d\kappa_t \cdot \kappa_t \Phi_{n1}(\kappa_t) J_0 \left[\kappa_t \sqrt{\mu^{-2} \rho_x^2 + \mu^{-2} \rho_y^2} \right], \quad (47)$$

with

$$\kappa_t = \left| (\mu \kappa_x, \mu \kappa_y)^\top \right|. \quad (48)$$

4.1.2. B. Wave structure function of spherical wave

Next, based on the 2nd-order statistical moments given above, we derive the WSF of a spherical wave in the non-Kolmogorov oceanic optical turbulence. According to the expressions in chapter 6 of [42] the WSF of a spherical wave has form:

$$\begin{aligned} D_{sp}(\boldsymbol{\rho}, L) &= \text{Re} [\Delta(\boldsymbol{\rho}, L)] = E_2(\mathbf{r}_1, \mathbf{r}_1) + E_2(\mathbf{r}_2, \mathbf{r}_2) - 2E_2(\mathbf{r}_1, \mathbf{r}_2) \\ &= 2E_2(\mathbf{0}) - 2E_2(\boldsymbol{\rho}), \end{aligned} \quad (49)$$

where E_2 is the 2nd-order statistical moment of a spherical wave. In combining with Eq. (45), we find that the WSF of a spherical wave in a horizontal channel ($\boldsymbol{\rho} = (\rho_x, \rho_z)$) takes form

$$D_{sp_h}(\boldsymbol{\rho}, L) = \frac{8\pi^2 k^2 \mu L}{n_0^2} \int_0^{+\infty} d\kappa_{\text{iso}} \cdot \kappa_{\text{iso}} \Phi_{n1}(\kappa_{\text{iso}}) \left[1 - J_0 \left(\kappa_{\text{iso}} \sqrt{\mu^{-2} \rho_x^2 + \rho_z^2} \right) \right]. \quad (50)$$

Similarly, the WSF of a spherical wave in a vertical channel ($\boldsymbol{\rho} = (\rho_x, \rho_y)$) becomes

$$D_{sp_v}(\boldsymbol{\rho}, L) = \frac{8\pi^2 k^2 L}{n_0^2} \int_0^{+\infty} d\kappa_{\text{iso}} \cdot \kappa_{\text{iso}} \Phi_{n1}(\kappa_{\text{iso}}) \left[1 - J_0 \left(\kappa_{\text{iso}} \sqrt{\mu^{-2} \rho_x^2 + \mu^{-2} \rho_y^2} \right) \right]. \quad (51)$$

When $\mu = 1$, the WSFs in horizontal and vertical channels are equal and, hence,

$$D_{sp_h}(\boldsymbol{\rho}, L) = D_{sp_v}(\boldsymbol{\rho}, L) = \frac{8\pi^2 k^2 L}{n_0^2} \int_0^{+\infty} d\kappa \cdot \kappa \Phi_{n1}(\kappa) [1 - J_0(\kappa |\boldsymbol{\rho}|)]. \quad (52)$$

Equations (50) - (52) are the main results of this section. They characterize the WSF of a spherical wave in an anisotropic, non-Kolmogorov turbulence by means of single integrals. We first plot the numerical results of the WSFs in an isotropic turbulence, with different values of the power law exponents in Fig. 5, and then compare isotropic and anisotropic cases in Fig. 6. Figure 5 shows that the power-law exponents α_T and α_S have significant effects on the WSF. Such power laws can result in a much higher or lower WSF in the non-Kolmogorov case than that in the Kolmogorov case. Figure 6 shows that anisotropic turbulence leads to an anisotropic WSF which results in an elliptically shaped coherence radius, which we will further illustrate in the next section.

4.2. Coherence radius of a spherical wave

The coherence radius of a spherical wave can be directly employed for assessing the optical turbulence strength, and is also useful in calculating the statistics of various optical beams (e.g. [57]). It is defined as a transverse separation distance between two points in the propagating spherical wave that corresponds to the WSF's value of 2. As a rule, the coherence radius is considered to be a scalar quantity.

However, as we have shown in Section 4.1, the WSF could be anisotropic. Hence, here the 'coherence radius' is considered as a vector $\boldsymbol{\rho}_0$ and we define it as a *coherence radius vector* (CRV) $\boldsymbol{\rho}_0$ by setting

$$D_{sp}(\boldsymbol{\rho}_0, L) = 2. \quad (53)$$

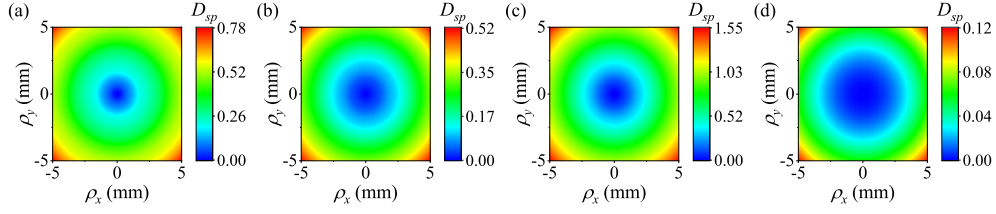


Fig. 5. The WSFs of spherical wave in isotropic turbulence ($\mu = 1$) with different values of power laws. (a) $(\alpha_T, \alpha_S) = (11/3, 11/3)$, (b) $(\alpha_T, \alpha_S) = (14/3, 11/3)$, (c) $(\alpha_T, \alpha_S) = (11/3, 14/3)$ and (d) $(\alpha_T, \alpha_S) = (14/3, 14/3)$. Values of other parameters are listed in Appendix II.

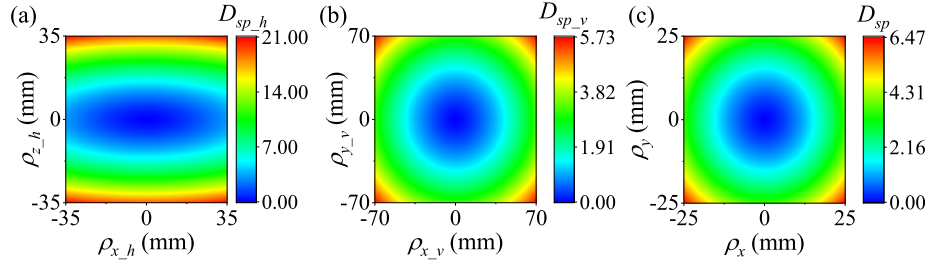


Fig. 6. The WSFs of spherical wave (a) in horizontal channels with $\mu = 3$, (b) in vertical channels with $\mu = 3$, and (c) in horizontal/vertical channels with $\mu = 1$. Values of other parameters are listed in Appendix II.

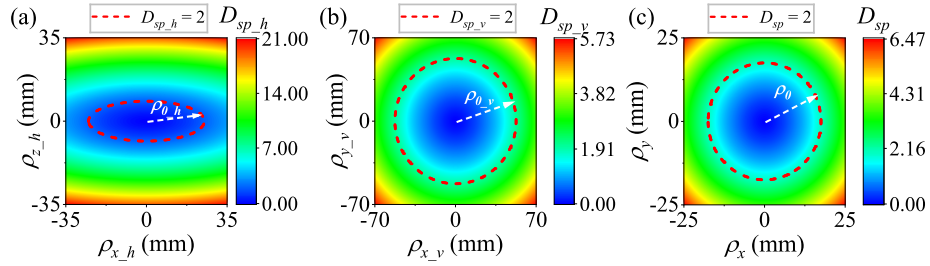


Fig. 7. The CRVs of (a) horizontal channel with $\mu = 3$, (b) vertical channel with $\mu = 3$, and (c) horizontal/vertical channel with $\mu = 1$. Values of other parameters are same as those of fig. 6.

For horizontal and vertical channels, we rewrite Eq. (53) as

$$D_{sp-h}(\rho_{0-h}, L) = 2, \quad D_{sp-v}(\rho_{0-v}, L) = 2, \quad (54)$$

where $\rho_{0-h} = (\rho_{0x-h}, \rho_{0z-h})^T$, $\rho_{0-v} = (\rho_{0x-v}, \rho_{0y-v})^T$ are the CRVs in horizontal channel and vertical channel, respectively.

A coherence radius scalar (CRS) ρ_{0-iso} is assumed as

$$\rho_{0-iso} = \begin{cases} \sqrt{\rho_{0x-h}^2 + \mu^2 \rho_{0z-h}^2} & \text{in horizontal channel,} \\ \sqrt{\rho_{0x-v}^2 + \rho_{0y-v}^2} & \text{in vertical channel.} \end{cases} \quad (55)$$

ρ_{0-iso} equals the widely used coherence radius if $\mu = 1$ or in vertical channel. Combining Eqs.

(50)-(51), (54) and (55), we have

$$\frac{8\pi^2 k^2 L}{n_0^2} \int_0^{+\infty} d\kappa \cdot \kappa \Phi_{n1}(\kappa) \left[1 - J_0 \left(\mu^{-1} \kappa \rho_{0_iso} \right) \right] = \begin{cases} 2\mu^{-1} & \text{for horizontal channels,} \\ 2 & \text{for vertical channels,} \end{cases} \quad (56)$$

where Φ_{n1} is the outer-scaled NK-OTOPS. Eqs. (55) and (56) can be used to predict the CRS ρ_{0_iso} and the CRV ρ_0 in oceanic turbulence. For example, according to Eqs. (39) and (56), ρ_{0_iso} in the cases of Figs. 6 (a)-(c) are 25.1mm, 52.5mm and 17.5mm, respectively; substituting ρ_{0_iso} into Eq.(55), we mark the CRVs by white arrows in Fig. 7.

The derived coherence radius vector (CRV) and scalar (CRS) are the main results of this section, which can be evaluated using Eqs. (55)-(56). The CRS corresponds to the widely used coherence radius if $\mu = 1$ or along a vertical channel, and it could measure the anisotropic turbulence strength along different directions. In fact, the atmospheric turbulence anisotropy has been recently directly assessed through a measurement of the elliptically shaped mutual coherence function of a laser beam [58] (see also a similar measurement via the elliptically shaped intensity-intensity correlation function [59]).

4.3. Co-effect of temperature and salinity on coherence radius scalar

In this section we will give a numerical example on the co-effect of temperature and salinity of the NK-OTOPS on the CRS by calculating it as a function of the power laws of temperature and salinity spectra α_T , α_S , as well as parameters c_T and c_S , defined by Eq. (6).

For brevity of discussion, we set the anisotropy constant $\mu = 3$ [60], and choose the CRS ρ_{0_iso} in vertical channels as a measurement of turbulent disturbance. The ranges of related parameters are listed as follows (see more details in Appendix. I):

$$\begin{aligned} & \cdot \alpha_T, \alpha_S \in [11/3, 15/3]; \\ & \cdot c_T \in [1.61 \times 10^{-3}, 3.99 \times 10^{-3}] \text{ and } c_S \in [9.76 \times 10^{-6}, 61.62 \times 10^{-6}]; \\ & \cdot C_S^2/C_T^2 \geq 3.18 \times 10^{-5} \text{ppt}^2 \cdot \text{deg}^{-2} \cdot \text{m}^{\alpha_T - \alpha_S}. \end{aligned}$$

Figure 8 shows $\rho_{0_iso}(\alpha_T, \alpha_S)$ and $\rho_{0_iso}(c_T, c_S)$ for different spectral correlation of the power spectrum (as above, fully correlated case refers to $\gamma_{ST} = 1$, partially correlated case refers to the γ_{ST} obeying Eq. (31), and uncorrelated case refers to $\gamma_{ST} = 0$, i.e. $\Phi_{TS} = 0$). Figure 8 (d) shows a distribution of $\rho_{0_iso}(\alpha_T, \alpha_S)$ being very different from that in Figs. 8 (a)-(c), and Fig. 8 (e) shows a distribution of $\rho_{0_iso}(c_T, c_S)$ being very different from that in Figs. 8 (f)-(h).

Figure 9 shows $\rho_{0_iso}(\alpha_T, \alpha_S)$ and $\rho_{0_iso}(c_T, c_S)$ with different ratios of C_S^2 to C_T^2 . With the increase of C_S^2/C_T^2 , the variation of ρ_{0_iso} with α_S and c_S becomes more pronounced.

A comprehensive analysis of Figs. 8 and 9 reveals that

- ρ_{0_iso} substantially varies with α_T and α_S (can reach an order of difference magnitude).
- $\gamma_{ST}(\kappa\eta)$, as a function describing the correlation between temperature and salinity spectra, has an obvious effect on ρ_{0_iso} .
- As expected, the structure constant C_T^2 or/and C_S^2 describes the contribution of temperature or/and salinity fluctuation very well.

5. Summary and conclusion

The power spectrum of refractive-index fluctuations provides a rigorous physical description of the 2nd-order statistics of natural random media, hence, bearing utmost significance for

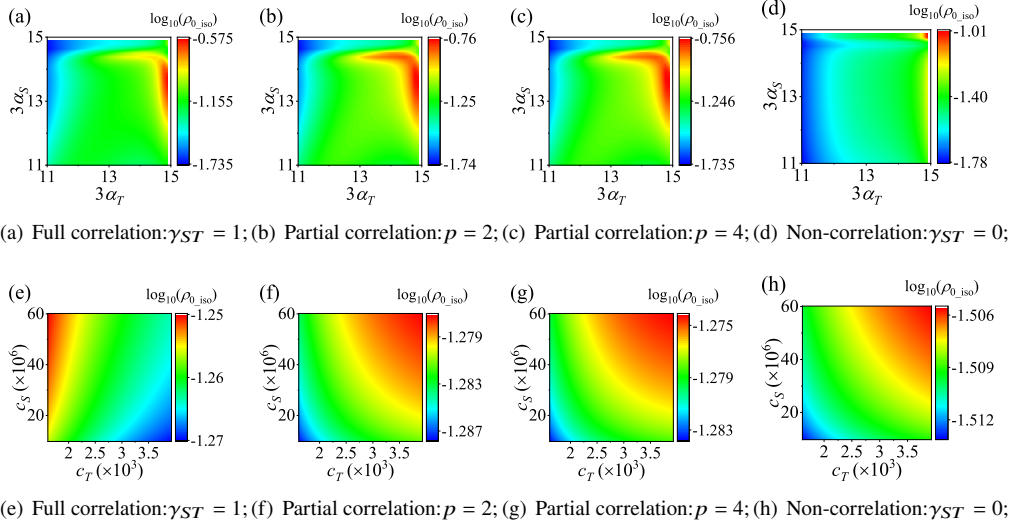


Fig. 8. The distributions $\rho_{0_iso}(\alpha_T, \alpha_S)$ and $\rho_{0_iso}(c_T, c_S)$ with different spectral correlation γ_{ST} . Values of parameters are listed in Appendix II. Here α_T , α_S , c_T and c_S are dimensionless.

environmental optics. A number of non-Kolmogorov models have been recently developed for ‘single-diffuser’ turbulence, i.e., based on a single advected scalar, as is temperature in atmospheric case. However, to our knowledge, there was no model for non-Kolmogorov spectrum describing optical turbulence with two or more advected scalars, i.e., ‘double-diffuser turbulence’. The major obstacle for developing such a power spectrum was due to the fact that the co-spectrum of two scalar spectra in the non-Kolmogorov case could not be directly obtained by analogy with a method used for Kolmogorov case in which the power laws of the two scalar spectra are equal.

In this paper, we have developed for the first time a non-Kolmogorov power spectrum of oceanic refractive-index fluctuations, being an example of a double-diffuser, by deriving the temperature spectrum, the salinity spectrum, and their co-spectrum, based on the Upper-Bound limitation and on the concept of spectral correlation. Our developed spectrum generally handles non-Kolmogorov turbulence with partially correlated temperature-salinity co-spectrum ($\alpha_i \in [11/3, 15/3]$ and $\gamma_{ST}(\kappa) \leq 1$) which is common for the stratified flow fields, but reduces to conventional, Kolmogorov spectrum, with fully correlated co-spectrum ($\alpha_i = 11/3$ and $\gamma_{ST} = 1$). We have also provided the extension to anisotropic non-Kolmogorov turbulence case.

Besides, we have also illustrated how a non-Kolmogorov, isotropic and anisotropic oceanic turbulence affects the second-order statistics of a spherical wave. The numerical calculations have revealed that the turbulence’s effect on a spherical wave substantially varies with the power law exponents (α_T and α_S). Moreover, we have shown for the first time that the coherence radius scalar ρ_{0_iso} takes on very different values for different settings of spectral correlation. This also indicates the usefulness of developing the oceanic non-Kolmogorov power spectrum with correlation factor γ_{ST} .

The numerical calculations in this manuscript focus on the coherence radius of a spherical wave. They are done for showing the significance of several parameters, like the non-Kolmogorov power law α_i and the correlation factor γ_{ST} (they do change the coherence radius a lot). A further significant work is to obtain simple analytical formulae of coherence radius. This could be done with approximations and simplifying OTOPS. The readers can access the codes of numerical results at the link [<https://github.com/jinry2017/Arxiv200902447>].

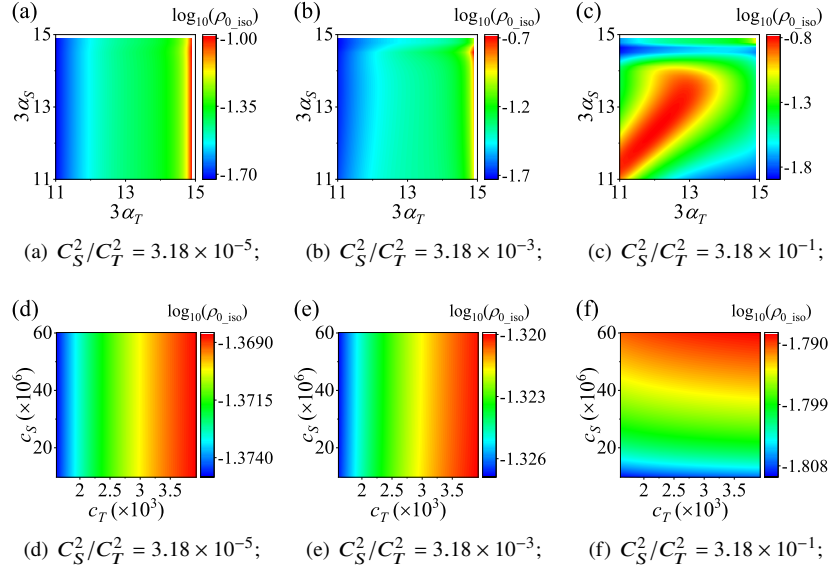


Fig. 9. The distributions $\rho_{0_iso}(\alpha_T, \alpha_S)$ and $\rho_{0_iso}(c_T, c_S)$ with different values of C_S^2/C_T^2 . All C_S^2/C_T^2 has the unit $\text{ppt}^2\text{deg}^{-2}\text{m}^{\alpha_T-\alpha_S}$. α_T, α_S, c_T and c_S are dimensionless. Values of parameters are listed in Appendix II.

On finishing we mention that so far no literature of oceanic turbulence has provided models for the correlation factor $\gamma_{ST}(\kappa)$ and other parameters such as c_T, c_S, α_T and α_S . But like in the studies of atmospheric propagation, these parameters could be significant in characterizing oceanic optical turbulence, and any details about them are of importance for further experimental campaigns. Our model fills such a gap by providing a rather simple analytical model applicable in a variety of oceanic turbulence regimes.

Appendix I. Ranges of parameters

For brevity of numerical calculation, we set the ranges of parameters as follows. *The ranges here are based on references, and some of them are obtained in Kolmogorov case. The real ranges could be beyond what we set.*

1. Constants

As given in [2, 18, 61], $a = 0.072$, $\beta = 0.72$ and $Q = 2.73$.

2. The ranges of α_T and α_S

According to the experimental data in [40] and the widely used range [32], non-Kolmogorov parameter $\alpha_i \in [11/3, 15/3]$.

3. The range of C_S^2/C_T^2

According to Eq. (2),

$$C_S^2/C_T^2 = \chi_S/\chi_T, \quad (57)$$

where the dissipation rate χ_i of temperature and salinity are related through [17, 22]

$$\chi_S/\chi_T = d_r H^{-2}, \quad (58)$$

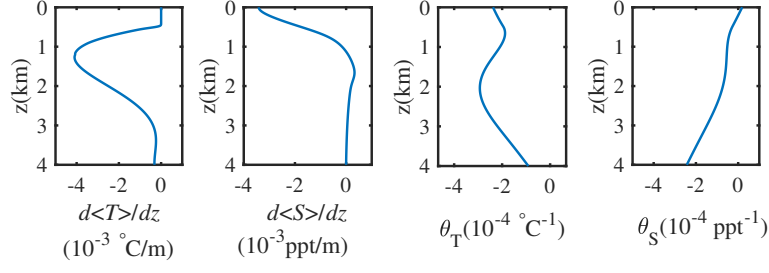


Fig. 10. The distribution of temperature gradient $d\langle T\rangle/dz$, salinity gradient $d\langle S\rangle/dz$, thermal expansion coefficient θ_T and saline contraction coefficient θ_S varying with depth z in Pacific.

with

$$d_r \approx \begin{cases} |H\theta_T\theta_S^{-1}| + |H\theta_T\theta_S^{-1}|^{0.5}(|H\theta_T\theta_S^{-1}| - 1)^{0.5}, & |H\theta_T\theta_S^{-1}| \geq 1, \\ 1.85|H\theta_T\theta_S^{-1}| - 0.85, & 0.5 \leq |H\theta_T\theta_S^{-1}| < 1, \\ 0.15|H\theta_T\theta_S^{-1}|, & |H\theta_T\theta_S^{-1}| < 0.5, \end{cases} \quad (59)$$

where d_r is the eddy diffusivity ratio, θ_T and θ_S are the thermal expansion coefficient and the saline contraction coefficient, respectively, and H is the temperature-salinity gradient ratio defined by

$$H = \frac{d\langle T\rangle/dz}{d\langle S\rangle/dz}. \quad (60)$$

Combining Eqs.(57)-(60), we have

$$\frac{C_S^2}{C_T^2} = \begin{cases} |H^{-1}\theta_T\theta_S^{-1}| + |H^{-1}\theta_T\theta_S^{-1}|(1 - |H^{-1}\theta_S\theta_T^{-1}|)^{0.5}, & |H\theta_T\theta_S^{-1}| \geq 1 \\ 1.85|H^{-1}\theta_T\theta_S^{-1}| - 0.85|H|^{-2}, & 0.5 \leq |H\theta_T\theta_S^{-1}| < 1 \\ 0.15|H^{-1}\theta_T\theta_S^{-1}|, & |H\theta_T\theta_S^{-1}| < 0.5 \end{cases} \quad (61)$$

Using the data of $d\langle T\rangle/dz$, $d\langle S\rangle/dz$, θ_T and θ_S of mid latitude Pacific in winter [62] (see also Fig. 10), and based on Eq. (61), we plot C_S^2/C_T^2 as a function of depth in Fig. 11. It shows that

$$C_S^2/C_T^2 \geq 3.18 \times 10^{-5} \text{ppt}^2 \cdot \text{deg}^{-2}. \quad (62)$$

For non-Kolmogorov cases, we assume

$$C_S^2/C_T^2 \geq 3.18 \times 10^{-5} \text{ppt}^2 \cdot \text{deg}^{-2} \cdot \text{m}^{\alpha_T - \alpha_S}. \quad (63)$$

4. The ranges of c_S and c_T

According to [22], Pr_T varies from 5.4 to 13.4, and Pr_S varies from 350.0 to 2210.0. Using the relation in Eq.(6) with constants $a = 0.072$ and $\beta = 0.72$, we have

$$c_T \in [1.61 \times 10^{-3}, 3.99 \times 10^{-3}] \quad \text{and} \quad c_S \in [9.76 \times 10^{-6}, 61.62 \times 10^{-6}]. \quad (64)$$

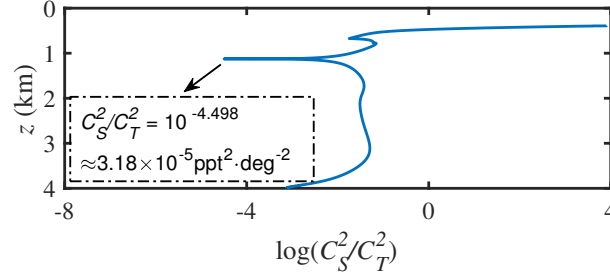


Fig. 11. The distribution of C_S^2/C_T^2 [ppt²deg⁻²m ^{$\alpha_T - \alpha_S$}] varying with depth z in Pacific.

Appendix II. The values of parameters in Figures

Here we list the values of parameters in figures.

- Figure 3: $\alpha_T = \alpha_S = 11/3$, $c_T = 2.6 \times 10^{-3}$, $c_S = 2.63 \times 10^{-5}$.
- Figure 5: $c_T = 2.63 \times 10^{-3}$, $c_S = 2.55 \times 10^{-5}$, $C_T^2 = 1.74 \times 10^{-4} \text{deg}^2 \text{m}^{3-\alpha_T}$, $C_S^2 = 7.67 \times 10^{-6} \text{ppt}^2 \text{m}^{3-\alpha_S}$, $\eta = 2.02 \times 10^{-4} \text{m}$, $\lambda_0 = 532 \text{nm}$, $n'_T = -8.84 \times 10^{-5} \text{deg}^{-1}$, $n'_S = 1.87 \times 10^{-4} \text{g}^{-1}$, $L = 15 \text{m}$, $L_0 = 30 \text{m}$.
- Figure 6: $\alpha_T = 14/3$, $\alpha_S = 11/3$, $c_T = 2.63 \times 10^{-3}$, $c_S = 2.55 \times 10^{-5}$, $C_T^2 = 1.74 \times 10^{-4} \text{deg}^2 \text{m}^{3-\alpha_T}$, $C_S^2 = 7.67 \times 10^{-6} \text{ppt}^2 \text{m}^{3-\alpha_S}$, $\eta = 2.02 \times 10^{-4} \text{m}$, $\lambda_0 = 532 \text{nm}$, $n'_T = -8.84 \times 10^{-5} \text{deg}^{-1}$, $n'_S = 1.87 \times 10^{-4} \text{g}^{-1}$, $L = 15 \text{m}$, $L_0 = 30 \text{m}$.
- Figure 7: same as those values in Fig. 6.
- Figure 8: $C_T^2 = 1.74 \times 10^{-4} \text{deg}^2 \text{m}^{3-\alpha_T}$, $C_S^2 = 7.67 \times 10^{-6} \text{ppt}^2 \text{m}^{3-\alpha_S}$, $\lambda_0 = 532 \text{nm}$, $n'_T = -8.84 \times 10^{-5} \text{deg}^{-1}$, $n'_S = 1.87 \times 10^{-4} \text{g}^{-1}$, $L = 15 \text{m}$, $L_0 = 30 \text{m}$, and $\eta = 2.02 \times 10^{-4} \text{m}$. (a)-(c) are plotted with $(c_T, c_S) = (2.63 \times 10^{-3}, 2.55 \times 10^{-5})$, and (d)-(e) are plotted with $(\alpha_T, \alpha_S) = (14/3, 11/3)$.
- Figure 9: $C_T^2 = 1.74 \times 10^{-4} \text{deg}^2 \text{m}^{3-\alpha_T}$, $\lambda_0 = 532 \text{nm}$, $n'_T = -8.84 \times 10^{-5}$, $n'_S = 1.87 \times 10^{-4}$, $\eta = 2.02 \times 10^{-4}$, $L = 15 \text{m}$, $L_0 = 30 \text{m}$, γ is given by Eq. (31) with $p = 3$. (a)-(c) are plotted with $(c_T, c_S) = (2.63 \times 10^{-3}, 2.55 \times 10^{-5})$, and (d)-(e) are plotted with $(\alpha_T, \alpha_S) = (14/3, 11/3)$.

Appendix III. Terminologies

Here we list a brief explanation about some terminology in this manuscript.

- **Coherence radius vector (CRV) and coherence radius scalar (CRS):**
According to Section 4.1, the WSF D_{sp} in anisotropic turbulence could be also anisotropic. Hence, the coherence radius $|\rho_0|$ in $D_{sp}(\rho_0) = 2$ could vary with the orientation of ρ_0 . For brevity in discussion, we define ρ_0 as CRV, and define a scalar — CRS — in Eq. (55). The CRS equals coherence radius if $\mu = 1$ or in vertical channels.
- **Hill's model 1 (H1) and Hill's model 4 (H4):**
As widely accepted, the power spectrum of scalar fluctuations has two or three intervals [24]. For the turbulence with large Pr or Sc, there are three intervals: inertial-convective, viscous-convective and viscous-diffusive intervals. For the turbulence with small Pr or Sc, there are

two intervals: inertial and diffusive intervals. Hill's models provide continuous transition between different intervals. Hill's model 1 is mathematically analytic but not as precise as Hill's model 4, and Hill's model 4 is a non-linear differential equation that does not have a closed-form solution. By numerical fitting, some approximate models for ocean [19, 21] and atmosphere [63] have been proposed based on Hill's model 4.

- **H1-based and H4-based:**

They refer to the models based on Hill's model 1 and 4, respectively.

- **Upper-bound limitation:**

As proved in the Section 5.2.5 of [44], the co-spectrum ϕ_{ab} of scalars a and b are limited by

$$|\phi_{ab}|^2 \leq \phi_a \phi_b, \quad (65)$$

where ϕ_a and ϕ_b are the spectra of a and b , respectively.

- **spectral correlation, fully correlated, partially correlated and uncorrelated:**

The 'Correlation' in this manuscript refers to the correlation between temperature fluctuations and salinity fluctuations. The spectral correlation factor is defined as

$$\gamma_{ST} = \left[\frac{|\Phi_{TS}|^2}{\Phi_T \Phi_S} \right]^{1/2}, \quad (66)$$

where Φ_T and Φ_S are the 3-D spectra of temperature and salinity, respectively. 'fully correlated' and 'full correlation' refer to the cases of $\gamma_{ST} = 1$; 'partially correlated' and 'partial correlation' refer to the cases of $\gamma_{ST} < 1$; 'uncorrelated' and 'non-correlation' refer to the cases of $\gamma_{ST} = 0$.

Disclosures

The authors declare no conflicts of interest.

References

1. O. Korotkova, "Light propagation in a turbulent ocean," in *Progress in Optics*, vol. 64 (Elsevier, 2019), pp. 1–43.
2. V. V. Nikishov and V. I. Nikishov, "Spectrum of turbulent fluctuations of the sea-water refraction index," *Int. J. Fluid Mech. Res.* **27**, 82–98 (2000).
3. W. Lu, L. Liu, and J. Sun, "Influence of temperature and salinity fluctuations on propagation behaviour of partially coherent beams in oceanic turbulence," *J. Opt. A: Pure Appl. Opt.* **8**, 1052–1058 (2006).
4. E. Shchepakina, N. Farwell, and O. Korotkova, "Spectral changes in stochastic light beams propagating in turbulent ocean," *Appl. Phys. B* **105**, 415 (2011).
5. O. Korotkova and N. Farwell, "Effect of oceanic turbulence on polarization of stochastic beams," *Opt. Commun.* **284**, 1740–1746 (2011).
6. N. Farwell and O. Korotkova, "Intensity and coherence properties of light in oceanic turbulence," *Opt. Commun.* **285**, 872–875 (2012).
7. O. Korotkova, N. Farwell, and E. Shchepakina, "Light scintillation in oceanic turbulence," *Waves Random Complex Media* **22**, 260–266 (2012).
8. Y. Baykal, "Scintillation index in strong oceanic turbulence," *Opt. Commun.* **375**, 15–18 (2016).
9. Y. Ata and Y. Baykal, "Structure functions for optical wave propagation in underwater medium," *Waves Random Complex Media* **24**, 164–173 (2014).
10. L. Lu, X. Ji, and Y. Baykal, "Wave structure function and spatial coherence radius of plane and spherical waves propagating through oceanic turbulence," *Opt. Express* **22**, 27112–27122 (2014).
11. O. Korotkova, "Enhanced backscatter in lidar systems with retro-reflectors operating through a turbulent ocean," *J. Opt. Soc. Am. A* **35**, 1797–1804 (2018).
12. Y. Baykal, "Bit error rate of pulse position modulated optical wireless communication links in oceanic turbulence," *J. Opt. Soc. Am. A* **35**, 1627–1632 (2018).
13. X. Yi, Z. Li, and Z. Liu, "Underwater optical communication performance for laser beam propagation through weak oceanic turbulence," *Appl. Opt.* **54**, 1273–1278 (2015).

14. Z. Cui, P. Yue, X. Yi, and J. Li, "Scintillation of a partially coherent beam with pointing errors resulting from a slightly skewed underwater platform in oceanic turbulence," *Appl. optics* **58**, 4443–4449 (2019).
15. W. W. Hou, "A simple underwater imaging model," *Opt. letters* **34**, 2688–2690 (2009).
16. J. R. Yao, Y. Zhang, R. N. Wang, Y. Y. Wang, and X. J. Wang, "Practical approximation of the oceanic refractive index spectrum," *Opt. Express* **25**, 23283–23292 (2017).
17. M. Elamassie, M. Uysal, Y. Baykal, M. Abdallah, and K. Qaraqe, "Effect of eddy diffusivity ratio on underwater optical scintillation index," *J. Opt. Soc. Am. A* **34**, 1969–1973 (2017).
18. R. J. Hill, "Spectra of fluctuations in refractivity, temperature, humidity, and the temperature-humidity cospectrum in the inertial and dissipation ranges," *Radio Sci.* **13**, 953–961 (1978).
19. X. Yi and I. B. Djordjevic, "Power spectrum of refractive-index fluctuations in turbulent ocean and its effect on optical scintillation," *Opt. Express* **26**, 10188–10202 (2018).
20. Y. Li, Y. Zhang, and Y. Zhu, "Oceanic spectrum of unstable stratification turbulence with outer scale and scintillation index of gaussian-beam wave," *Opt. Express* **27**, 7656–7672 (2019).
21. J. R. Yao, H. J. Zhang, R. N. Wang, J. D. Cai, Y. Zhang, and O. Korotkova, "Wide-range prandtl/schmidt number power spectrum of optical turbulence and its application to oceanic light propagation," *Opt. Express* **27**, 27807–27819 (2019).
22. J. R. Yao, M. Elamassie, and O. Korotkova, "Spatial power spectrum of natural water turbulence with any average temperature, salinity concentration, and light wavelength," *J. Opt. Soc. Am. A* **37**, 1614–1621 (2020).
23. A. Muschinski and S. M. de Bruyn Kops, "Investigation of hill's optical turbulence model by means of direct numerical simulation," *J. Opt. Soc. Am. A* **32**, 2423–2430 (2015).
24. K. R. Sreenivasan, "Turbulent mixing: A perspective," *Proc. Natl. Acad. Sci.* **116**, 18175–18183 (2019).
25. M. S. Belen'kii, S. J. Karis, J. M. Brown II, and R. Q. Fugate, "Experimental study of the effect of non-kolmogorov stratospheric turbulence on star image motion," in *Adaptive Optics and Applications*, vol. 3126 (International Society for Optics and Photonics, 1997), pp. 113–123.
26. B. E. Stribling, B. M. Welsh, and M. C. Roggemann, "Optical propagation in non-kolmogorov atmospheric turbulence," in *Atmospheric Propagation and Remote Sensing IV*, vol. 2471 (International Society for Optics and Photonics, 1995), pp. 181–196.
27. D. T. Kyrazis, J. B. Wissler, D. D. Keating, A. J. Preble, and K. P. Bishop, "Measurement of optical turbulence in the upper troposphere and lower stratosphere," in *Laser Beam Propagation and Control*, vol. 2120 (International Society for Optics and Photonics, 1994), pp. 43–55.
28. L. J. Otten III, M. C. Roggemann, B. Al Jones, J. Lane, and D. G. Black, "High-bandwidth atmospheric-turbulence data collection platform," in *Optics in Atmospheric Propagation and Adaptive Systems III*, vol. 3866 (International Society for Optics and Photonics, 1999), pp. 23–32.
29. A. Zilberman, E. Golbraikh, and N. Kopeika, "Lidar studies of aerosols and non-kolmogorov turbulence in the mediterranean troposphere," in *Electro-Optical and Infrared Systems: Technology and Applications II*, vol. 5987 (International Society for Optics and Photonics, 2005), p. 598702.
30. A. Muschinski, "Non-kolmogorov turbulence," in *Imaging and Applied Optics 2017 (3D, AIO, COSI, IS, MATH, pcAOP)*, (Optical Society of America, 2017), p. PW2D.1.
31. I. Toselli, L. C. Andrews, R. L. Phillips, and V. Ferrero, "Angle of arrival fluctuations for free space laser beam propagation through non kolmogorov turbulence," in *Atmospheric Propagation IV*, vol. 6551 C. Y. Young and G. C. Gilbreath, eds., International Society for Optics and Photonics (SPIE, 2007), pp. 149 – 160.
32. I. Toselli, L. C. Andrews, R. L. Phillips, and V. Ferrero, "Free-space optical system performance for laser beam propagation through non-kolmogorov turbulence," *Opt. Eng.* **47**, 026003 (2008).
33. G. Wu, H. Guo, S. Yu, and B. Luo, "Spreading and direction of gaussian-schell model beam through a non-kolmogorov turbulence," *Opt. Lett.* **35**, 715–717 (2010).
34. E. Shchepakina and O. Korotkova, "Second-order statistics of stochastic electromagnetic beams propagating through non-kolmogorov turbulence," *Opt. Express* **18**, 10650–10658 (2010).
35. O. Korotkova and E. Shchepakina, "Color changes in stochastic light fields propagating in non-kolmogorov turbulence," *Opt. Lett.* **35**, 3772–3774 (2010).
36. A. Zilberman, E. Golbraikh, N. S. Kopeika, A. Virtser, I. Kupersmidt, and Y. Shtemler, "Lidar study of aerosol turbulence characteristics in the troposphere: Kolmogorov and non-kolmogorov turbulence," *Atmospheric Res.* **88**, 66–77 (2008).
37. I. Toselli, O. Korotkova, X. Xiao, and D. G. Voelz, "SIm-based laboratory simulations of kolmogorov and non-kolmogorov anisotropic turbulence," *Appl. Opt.* **54**, 4740–4744 (2015).
38. X. Xiao, D. G. Voelz, I. Toselli, and O. Korotkova, "Gaussian beam propagation in anisotropic turbulence along horizontal links: theory, simulation, and laboratory implementation," *Appl. Opt.* **55**, 4079–4084 (2016).
39. G. Funes, F. Olivares, C. G. Weinberger, Y. D. Carrasco, L. N. nez, and D. G. Pérez, "Synthesis of anisotropic optical turbulence at the laboratory," *Opt. Lett.* **41**, 5696–5699 (2016).
40. T. Ichiye, "Power spectra of temperature and salinity fluctuations in the slope water off cape hatteras," *pure applied geophysics* **96**, 205–216 (1972).
41. T. E. Pochapsky and F. D. Malone, "Spectra of deep vertical temperature profiles," *J. Phys. Oceanogr.* **2**, 470–475 (1972).
42. R. L. Phillips, *Laser Beam Propagation through Random Media, Second Edition* (SPIE, 2005).

43. B. Xue, L. Cui, W. Xue, X. Bai, and F. Zhou, "Generalized modified atmospheric spectral model for optical wave propagating through non-kolmogorov turbulence," *JOSA A* **28**, 912–916 (2011).
44. B. Harris, "Random data: Analysis and measurement procedures," *Technometrics* **17**, 271–271 (1975).
45. L. Washburn, T. F. Duda, and D. C. Jacobs, "Interpreting conductivity microstructure: Estimating the temperature variance dissipation rate," *J. Atmospheric Ocean. Technol.* **13**, 1166–1188 (1996).
46. H. E. Seim, "Acoustic backscatter from salinity microstructure," *J. Atmospheric Ocean. Technol.* **16**, 1491–1498 (1999).
47. J. D. Nash and J. N. Moum, "Estimating salinity variance dissipation rate from conductivity microstructure measurements," *J. Atmospheric Ocean. Technol.* **16**, 263–274 (1999).
48. T. Ross, C. Garrett, and R. Lueck, "On the turbulent co-spectrum of two scalars and its effect on acoustic scattering from oceanic turbulence," *J. Fluid Mech.* **514**, 107–119 (2004).
49. In some references, the upper-bound model (Eq. (22)) was approximated as $\Phi_{TS} = (\Phi_T \Phi_S)^{1/2}$. In considering that the influence of this approximation on predicting light propagation is unknown, we adopt the concept of spectral correlation which provides elasticity under Upper-Bound limitation [47]. Examples of light propagation in fully correlated case, partially correlated case and uncorrelated case will be given in section 4.
50. The Prandtl number of temperature is much less than the Schmidt number of salinity, which leads to an asynchrony of the sub-ranges of Φ_T and Φ_S , i.e., asynchronous consumption of T' and S' . This asynchrony is responsible for the decrease of correlation which has been observed in numerical simulation [52].
51. Generally, salinity Schmidt number is so larger than temperature Prandtl number that the inertial-convective range of salinity is wider than that of temperature. Hence, the salinity fluctuation is in its inertial-convective range if κ locates in the inertial-convective range of temperature spectrum.
52. P. K. Yeung, M. C. Sykes, and P. Vedula, "Direct numerical simulation of differential diffusion with schmidt numbers up to 4.0," *Phys. Fluids* **12**, 1601–1604 (2000).
53. The concept of spectral correlation has not been introduced into the H4-based temperature-salinity co-spectrum [21]. Here we calculate the γ_{ST} of traditional co-spectrum by calculating $\Phi_{TS}/(\Phi_T \Phi_S)^{1/2}$.
54. As shown in [22], n'_T and n'_S vary with environment (averaged temperature and salinity). Their variability also exists in non-Kolmogorov case. However, non-Kolmogorov case refers to inhomogeneous turbulence where the averaged temperature and salinity could change temporally and spatially. Hence, the variability of n'_T and n'_S is not clear for non-Kolmogorov case, and we will use fixed values in following numerical calculation for brevity.
55. V. V. Voitikhovich, "Outer scale of turbulence: comparison of different models," *J. Opt. Soc. Am. A* **12**, 1346–1353 (1995).
56. I. Toselli, "Introducing the concept of anisotropy at different scales for modeling optical turbulence," *J. Opt. Soc. Am. A* **31**, 1868–1875 (2014).
57. O. Korotkova and J.-R. Yao, "Bi-static lidar systems operating in the presence of oceanic turbulence," *Opt. Commun.* **460**, 125119 (2020).
58. C. Wu, D. A. Paulson, J. R. Rzasa, and C. C. Davis, "Light field camera study of near-ground turbulence anisotropy and observation of small outer-scales," *Opt. Lett.* **45**, 1156–1159 (2020).
59. F. Wang, I. Toselli, J. Li, and O. Korotkova, "Measuring anisotropy ellipse of atmospheric turbulence by intensity correlations of laser light," *Opt. Lett.* **42**, 1129–1132 (2017).
60. The anisotropic factor μ was firstly introduced into OTOPS in [64], where the range of μ is [1, 5]. Here we assume $\mu = 3$ for simplicity.
61. A. Muschinski and S. M. de Bruyn Kops, "Direct numerical simulation of isotropic and stratified optical turbulence," in *Propagation through and Characterization of Distributed Volume Turbulence and Atmospheric Phenomena*, (Optical Society of America, 2015), pp. PM4C–5.
62. R. Chester and T. D. Jickells, *Marine Geochemistry. Third edition* (Wiley-Blackwell, 2012).
63. L. C. Andrews, "An analytical model for the refractive index power spectrum and its application to optical scintillations in the atmosphere," *J. Mod. Opt.* **39**, 1849–1853 (1992).
64. Y. Baykal, "Effect of anisotropy on intensity fluctuations in oceanic turbulence," *J. Mod. Opt.* **65**, 825–829 (2018).